Applied Physics Letters ARTICLE pubs.aip.org/aip/apl

Limiting role of dislocations in high-current AlGaN/GaN hot electron transistors

Cite as: Appl. Phys. Lett. **124**, 063505 (2024); doi: 10.1063/5.0193571
Submitted: 22 December 2023 · Accepted: 24 January 2024 ·
Published Online: 6 February 2024

J. W. Daulton,[1,2,a)] R. J. Molnar,[1] J. A. Brinkerhoff,[1] T. J. Weir,[1] M. A. Hollis,[1] and A. Zaslavsky[2]

AFFILIATIONS

[1]MIT Lincoln Laboratory, Lexington, Massachusetts 02142, USA
[2]School of Engineering, Brown University, Providence, Rhode Island 02912, USA

[a)]Author to whom correspondence should be addressed: Jeffrey_Daulton@brown.edu

ABSTRACT

III-nitride-based hot electron transistors (HETs) hold significant promise as high-speed, high-power devices. In our previous work, we demonstrated high current density and common-emitter gain at room temperature. Here, we measure multiple devices at cryogenic temperatures, extending the Gummel characteristics past the onset of intervalley scattering at 77 K. We demonstrate a Gummel current gain of 4.7 at a collector current density of 2.6 MA/cm^2 at 77 K as well as a peak current density exceeding 3 MA/cm^2. From these data, we determine that dislocation-associated inhomogeneities play a limiting role in AlGaN/GaN HETs, controlling the current gain, density, knee voltage, and base-collector leakage. A comparison of two nominally identical devices suggests that even a modest reduction in dislocation density would result in a substantial improvement in HET performance.

Gallium arsenide-based hot electron transistors (HETs), where energetic electrons are injected into a base layer, which they traverse ballistically before surmounting the base-collector (BC) barrier, attracted significant research effort throughout the 1980s.[1–4] However, the low Γ to L intervalley energy spacing in GaAs, which limited ballistic transport and gain, eventually caused interest in these devices to wane. Most exploration of GaAs-based devices involved cryogenic operation,[1–3] with only limited later work showing reasonable gain at 300 K.[4,5] More recently, progress in III-nitride materials has caused a resurgence of interest in such devices,[6–9] as the large intervalley Γ to M-L energy separation of ∼2 eV of III-nitride materials allows for significantly higher injected electron energy E_{inj} before the onset of intervalley scattering. However, until recently, reported devices had relatively low current density and gain, including devices grown on bulk GaN,[7,8] with minimal difference between identical structures grown on sapphire and bulk GaN.[7] Additionally, the behavior of these devices at cryogenic temperatures had remained unexplored, with only limited temperature-dependent studies in nitride HETs appearing in the literature.[10] For completeness, we note that HETs with graphene base layers have also been reported, but the ultra-thin bases have not resulted in high gain or high current density.[11–13]

We previously reported on room-temperature GaN-based HETs exhibiting high common-emitter current gain $\beta = I_C/I_B > 20$ and high current density $I_C > 440$ kA/cm^2.[14] In our design, the electron beam is collimated by injecting into the base from a 2D quantized subband formed in the emitter, with the base doped via polarization only. This approach eliminates the ionized impurity scattering that significantly reduced electron mean-free path in most earlier demonstrations. More recently, we repeated DC testing of our devices at 77 and 4.2 K, demonstrating minimal temperature sensitivity in both transistor I–V characteristics and transfer coefficient $\alpha = I_C/I_E$, indicating a dominant role of LO-phonon emission in scattering within the GaN base region.[15] Now, we have also extended the testing to additional devices to examine the impact of dislocations on device behavior, as well as demonstrating $I_C > 3$ MA/cm^2 at 77 K ambient by immersion in liquid N_2.

A schematic cross section of the fabricated device is shown in Fig. 1(a) together with a top view of the device, with emitter and base contacts and base mesa outlined (vertical dashed lines indicate the cut-lines for technology computer-aided design (TCAD) simulations later in the text). Design simulations were carried out in Synopsys Sentaurus[16] to confirm the formation of a triangular quantum well in the emitter and a high-density 2D electron gas (2DEG) in the base, with electron injection energy from the lowest quantized subband in the emitter not to exceed the Γ to M-L intervalley energy spacing under active biasing. The epitaxial structure was grown by MOCVD (metalorganic chemical vapor deposition) on 2 in. sapphire wafers after

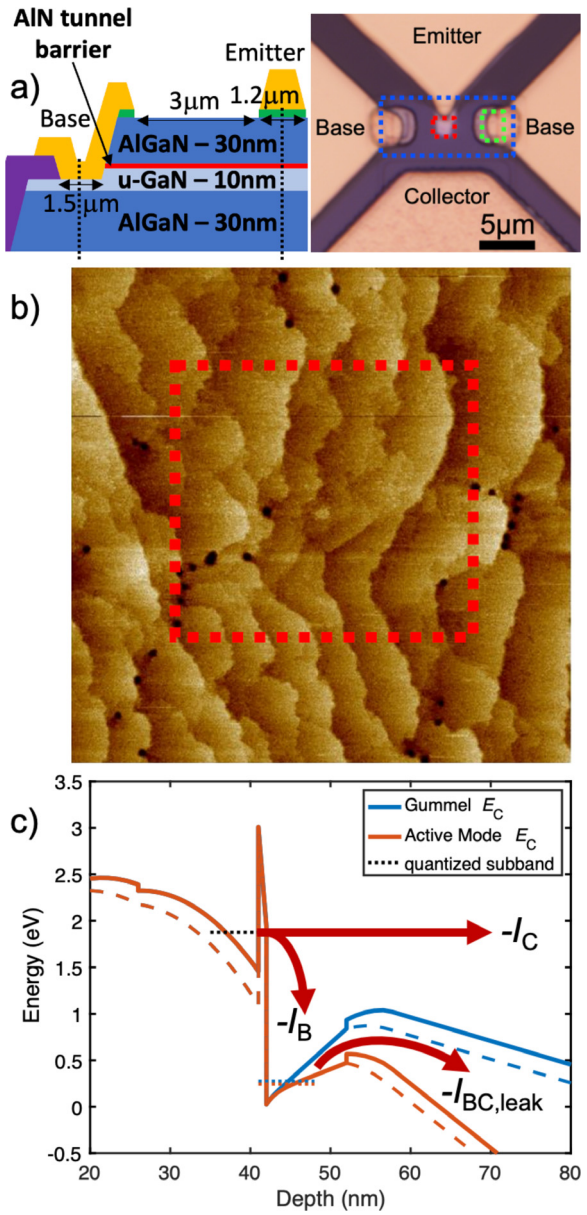

FIG. 1. (a) Device cross section and top-view microscope image of a HET, showing emitter area (red), base mesa area (blue), and base contact area (green); dashed lines indicate cut lines under the emitter and base contacts used in later simulations; (b) AFM image of epitaxial surface after growth, with ~1.3 μm^2 emitter area indicated (red), with several dislocations visible; (c) self-consistent emitter-base conduction band diagram at $V_{BE} = 2$ V, $V_{CB} = 0$ V (blue) and $V_{CB} = 2$ V (orange), showing the lowest 2D subbands in the emitter and base (dotted lines) and the GaN conduction band in the emitter and collector (dashed lines). Arrows show electron flow components, including the base-collector leakage $I_{BC,leak}$.

growth of a ~4 μm GaN buffer, with 2 × 2 μm atomic force microscopy (AFM) scan of the post-growth surface shown in Fig. 1(b), showing a dislocation density of ~5×10^8 cm^{-2}, typical of growth on sapphire.[9] The emitter stack consisted of a ~10^{19} cm^{-3} doped emitter cap, with a triangular quantum well formed by polarization fields in the undoped graded AlGaN emitter next to an ultrathin 1.5 nm AlN tunnel barrier. The narrow $W_B = 10$ nm GaN base is undoped, with a 2DEG density of ~3.5×10^{12} cm^{-2} formed by polarization doping. The collector region consisted of a graded AlGaN base-collector transition layer to an $Al_{0.12}Ga_{0.88}N$ collector barrier. The resulting band diagram, including the quantized injection subband in the emitter and the I_C and I_B electron flow components, as well as base-collector leakage $I_{BC,leak}$, is shown in Fig. 1(c). Fabrication details, including damage-free BCl_3/O_2 atomic layer etching[17] for low-resistance sidewall contacts to the 2DEG in the base, as well as contact metallization and isolation steps (including PECVD SiO_2 sidewall passivation), are available in our earlier work.[14] Such a structure, where currents are kept away from semiconductor/dielectric interfaces and that is realized entirely by pseudomorphic heteroepitaxial growth, limits the impact of traps.[12]

Figure 1(c) also shows the approximate GaN conduction band edge E_C within the AlGaN regions (dashed lines), because, as we discuss later, this represents the most extreme local stoichiometry fluctuation that would affect device characteristics. Actual values of E_C are expected to deviate from this locally due to fluctuating vertical polarization dipoles at AlGaN/GaN and AlGaN/AlN interfaces, as has been observed around dislocations in GaN HEMTs.[18]

Figure 2(a) presents the transfer coefficient α of three nominally identical HETs at 300 K measured under Gummel condition ($V_{CB} = 0$), with α increasing rapidly from device turn-on, indicating the onset of ballistic transport through the base. Devices that see the highest α values also see the sharpest initial increase in α and the differences between the curves for $V_{BE} > 2$ V remain generally constant. Figure 2(b) shows 77 K Gummel results for devices T1 and T2 (device T3 with the best α was damaged during wire bonding) for I_C, α, and dI_C/dI_E. Sharpening of the initial increase in α is observed, as would be expected from delayed thermionic filling of the emitter quantum well. Device T1 reaches $I_{C,max}$ ~3.1 MA/cm^2 with $g_{m,max} = dI_C/dV_{BE}$ ~1.4 MS/cm^2, with maximum $\alpha = 0.824$ ($\beta = 4.7$). The maximum value on the $\Delta\alpha$ curves indicates the onset of intervalley transfer V_{tr}.[19] This acts as a convenient internal bias reference for the device. While these values of I_C and α exceed values of previous reports of III-N HETs at 300 K[7–9,14] and 77 K,[10,15] further improvements are necessary for practical devices that require higher β, ideally >20 under Gummel conditions.

The transfer coefficient α can be expressed as $\alpha = \alpha_0 \exp[-W_B/\lambda_{MFP}]$, where $\alpha_0 < 1$ is the transfer coefficient for $W_B = 0$ nm.[20,21] Hot electron mean-free path λ_{MFP}, which exceeds 60 nm for our measured β given our $W_B = 10$ nm, should not vary significantly between devices due to minimal scattering by charged dislocations, as the dislocation lines are approximately parallel with the injected electrons. This suggests that the driver of differing α between devices is the off-normal or below-energy injection[3,22] contained within α_0, due to the presence of dislocations visible in Fig. 1(b).

Ideally, electrons are injected from a quantized subband in the emitter at large E_{inj}, creating a narrow angular distribution $\Delta\theta_{inj} \approx \tan^{-1}[(kT/E_{inj})^{1/2}] < 7°$, even at 300 K, but the various types of GaN dislocations introduce complications. For example, pure screw dislocations have been shown to behave as conductive leakage pathways,[23,24] but they represent only a small fraction (<10%) of dislocations in MOCVD-grown material, with the rest made up of either mixed or pure edge dislocations.[24,25] Since dislocations with a screw component have been shown to pin epitaxial terraces during growth, they are

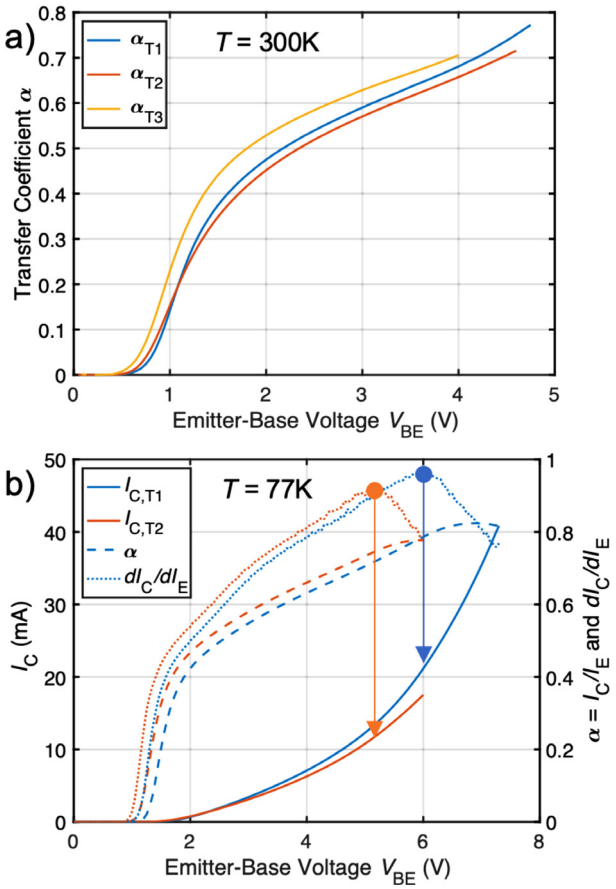

FIG. 2. (a) Transfer coefficient α as a function of V_{BE} for three devices at 300 K under Gummel condition ($V_{CB} = 0$ V); (b) Gummel condition I_C, transfer coefficient α and $\Delta\alpha = dI_C/dI_E$ as a function of V_{BE} for devices T1 and T2 at 77 K, with V_{tr} marked for T1 ($I_C = 21.2$ mA, $\alpha = 0.787$, $\beta = 3.68$) and T2 ($I_C = 11.6$ mA, $\alpha = 0.745$, $\beta = 2.92$).

readily identifiable by AFM.[25] Taken in the context of Figs. 1(a) and 1(b), direct leakage through screw dislocations should not play a major role, since our material has a pure screw dislocation density $<0.5\,\mu m^{-2}$. However, dislocations have also been shown to impact local AlGaN stoichiometry through a variety of mechanisms, with the most extreme variation localized around a dislocation core,[26] but still significant deviations of ±30% from the average composition of the layer.[27–29] This localized variation in film stoichiometry, when applied to the AlGaN quantum well emitter region, would be expected to create lateral (perpendicular to the *c*-axis) electric fields on the order of 1 MV/cm, leading to large-angle (>45°) off-normal injection from the emitter quantized subband into the base, increasing the base path length and scattering rate.[1,30] Furthermore, the size of these compositional distortions implies that the local E_C and the emitter subband energy vary considerably, broadening E_{inj} and θ_{inj} distributions.[31,32] It may be observed from Fig. 1(c) that electrons injected from the GaN conduction band, or even some energy above it, are unlikely to surmount the collector barrier at Gummel condition ($V_{CB} = 0$). As a result, such electrons would necessarily become excess base current, limiting the Gummel gain $\beta = \alpha/(1 - \alpha) = I_C/I_B$ and output current I_C. Such behavior can be seen in Fig. 2(b), with the higher-gain device T1 showing a much higher I_C at V_{tr} than the increased gain alone would suggest. An analogous effect has been seen in GaN HBTs, where devices fabricated on free-standing GaN substrates exhibited ∼4× higher β but a much higher ∼7× I_C when compared to devices fabricated on sapphire substrates.[33]

Looking at the base from the perspective of electron continuity, the residence time of electrons becomes important. While electrons transiting the base ballistically only reside within the base region for $\tau_{tr} < 10$ fs, assuming a ballistic velocity $> 10^8$ cm/s for $E_{inj} > 1$ eV, electrons scattering to form I_B must be considered as resident within the base until they have relaxed into the 2DEG, a process that would be expected to occur over $\tau_{rel} > 100$ fs.[34] The resulting $n_{rel} = qJ_C\tau_{rel}/\beta W_B > 10^{19}\,cm^{-3} > n_{2DEG}/W_B$ places the base well into the space-charge limited regime. However, an assumption of the 2DEG as a metal is not entirely valid because these fully relaxed electrons will raise the base E_F slightly due to quantum capacitance effects,[35] reducing the effective bias of the emitter-base junction and increasing the effective base residence time for these electrons. This large differential in base residence times appears to play a significant role in the outsized increase in I_C for a relatively minor increase in α seen in Fig. 2(b) as the I_C curves separate at higher currents due to the increased impact of base space-charge impedance.

Figure 2 describes the Gummel condition; however, under normal operating mode, there is a $V_{CB} > 0$ as shown in Fig. 1(c), which leads to an unwanted $I_{BC,leak}$. All devices measured here exhibit excess leakage in the base-collector (BC) diode I_C–V_{CB} curve Fig. 3(a), exceeding the simulated I_C–V_{CB} curve by more than four orders of magnitude at low V_{CB}. This deviation arises from conduction mechanisms not accounted for within the TCAD model. An obvious candidate for this is conductivity along dislocations within the III-N crystal, with a pure screw dislocation density of $<0.5\,\mu m^{-2}$ allowing for significant device-to-device variation over the ∼60 μm^2 base mesa. This is consistent with the wide range of excess leakage current seen in the BC diode at low voltage at both 300 and 77 K in all three devices. In addition to this leakage mechanism, AlGaN compositional fluctuations have been shown to allow barrier permeability that reduces the effectiveness of the base-collector barrier in blocking base-collector leakage.[27] The diode I_C–V_{CB} characteristic of Fig. 3(a) in the $V_{CB} > 0$ range shows a visible inflection between $V_{CB} = 1.5$ and 2 V in devices T1 and T2 that is almost absent in device T3. The inflection in the *I*–*V* curves sharpens at 77 K in Fig. 3(b), notably occurring at the same V_{CB} bias point. It can be seen from the band diagram in Fig. 1(c) that the V_{CB} value at which this conductance step occurs aligns with the V_{CB} value where the approximate position of the GaN E_C within the collector-base AlGaN region no longer presents any additional potential barrier to current flow. We attribute this step in conductance to conduction through Al-depleted AlGaN around a dislocation core. From the combination of these proposed leakage mechanisms, we can infer that the relative dislocation counts within the emitter-base mesa between devices are such that dislocation count of T2 > T1 > T3, consistent with the relative ordering for α seen in Fig. 2(a).

Turning to the I_C–V_{CB} characteristic of Fig. 3(a) where $V_{CB} < 0$, there is onset of significant leakage at much lower bias than would be suggested by the TCAD model. This low turn-on voltage is only minimally increased under 77 K operation [Fig. 3(b)]. Conduction band

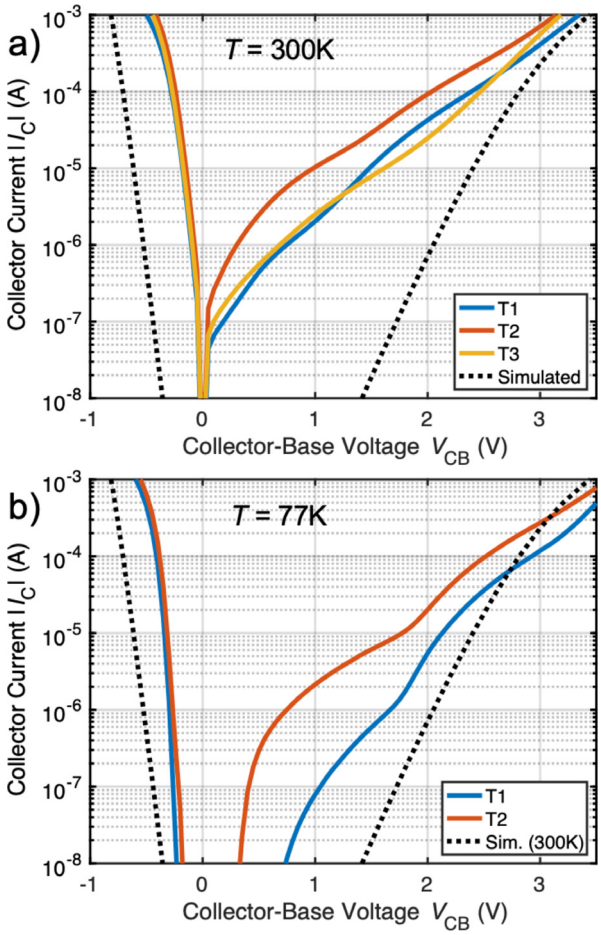

FIG. 3. (a) Base-collector diode I_C–V_{CB} characteristics for devices T1, T2, and T3 at 300 K with comparison to TCAD simulation; (b) base-collector diode I_C–V_{CB} for T1 and T2 at 77 K (with 300 K simulation shown by dashed line as guide to the eye).

diagrams of slices through the emitter and base [along cutlines shown in Fig. 1(a)] are shown in Fig. 4, with $-I_{BC,leak}$ indicated. From these, it can be observed that the collector-base barrier is suppressed by the depth of the base contact placement in the GaN base layer. This suggests that, unlike the forward portion of the BC diode I_C–V_{CB} curve, this region is dominated by the behavior of the base contact area, with a particular sensitivity to base contact etch depth. The approximate GaN E_C position in the AlGaN with respect to E_F within the collector is consistent with the early turn-on behavior, as the modeled uniform AlGaN E_C would be expected to still present a significant energy barrier at such voltages. The delayed turn-on for devices T1 and T3 with respect to T2 is consistent with higher dislocation count within the area of device T2 and, when combined with band diagram slices and the model of AlGaN segregation around dislocations, appears to be a reasonable interpretation for this early turn-on behavior. An unfortunate consequence of the high $I_{BC,leak}$ on these devices is that it prevents spectrometer-mode operation of the HET,[3] where the collector is biased such that $V_{CB} < 0$ in order to raise the barrier height and study the injected hot electron distribution.

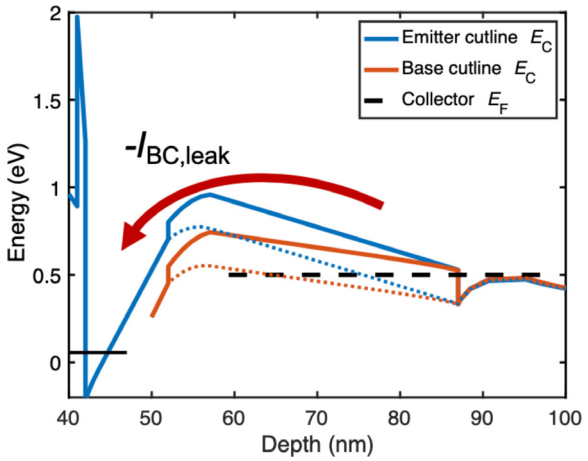

FIG. 4. Simulated base-collector band diagrams at 300 K for $V_{CB} = -0.5$ V with estimated GaN E_C (dotted) for cuts below the emitter and base contacts [see Fig. 1(a)], with base 2D subband and $-I_{BC,leak}$ indicated.

The 77 K common-emitter characteristic for device T1 at $V_{BE} = 3$ V is shown in Fig. 5(a) together with the measured $I_{BC,diode}$–V_{CB} diode characteristic. For analyzing the relationship between these curves, the $I_{BC,diode}$–V_{CB} curve is then shifted upward (dashed line) so that it intersects the common-emitter curve at the Gummel point. The vertical line denotes the knee voltage V_{knee} in the common-emitter I_C. The full common-emitter characteristics for device T1 are shown for 300 K in Fig. 5(b) and for 77 K in Fig. 5(c), with overlaid $I_{BC,diode}$ curves for $V_{CB} < 0$, with the same V_{knee} reference line as in Fig. 5(a). From the agreement between the common-emitter V_{knee} and the turn-on for the BC diode at both temperatures and the sharpening of the knee at low T as in the $I_{BC,diode}$–V_{CB} curves, it is clear that the knee voltage is not defined by the turn-off of ballistic current into the collector, but by this current component being canceled out by $I_{BC,leak}$, which is clearly dominated by $I_{BC,diode}$. The output conductance g_D, seen as the slope of the active region of the common emitter curves, may be understood as a function of increased collection of electrons passing over a lowered collector barrier with increased bias,[3] as well as the slight penetration of the electric field through the base 2DEG.[35] Narrower E_{inj} and θ_{inj} distributions, expected from more ideal behavior of the quantum-confined emitter in the absence of dislocations, would flatten this portion of the common-emitter curves, reducing g_D and simultaneously increasing the current gain β. These expected improvements in current density, gain, knee voltage, and output conductance as a consequence of reduced dislocation density, as well as the increased thermal conductivity of free-standing GaN substrates, make the use of such substrates particularly attractive for future work.

In conclusion, we have fabricated high-current III-nitride hot electron transistors and characterized these devices at 300 and 77 K, using base-collector diode behavior as an indicator of relative dislocation density. From this indicator, we have extended the known impact of dislocations on material properties to explore their impact on relevant device parameters including current density, gain, output conductance, and knee voltage. We have also identified a mechanism for the outsized improvement in maximum current density imparted by

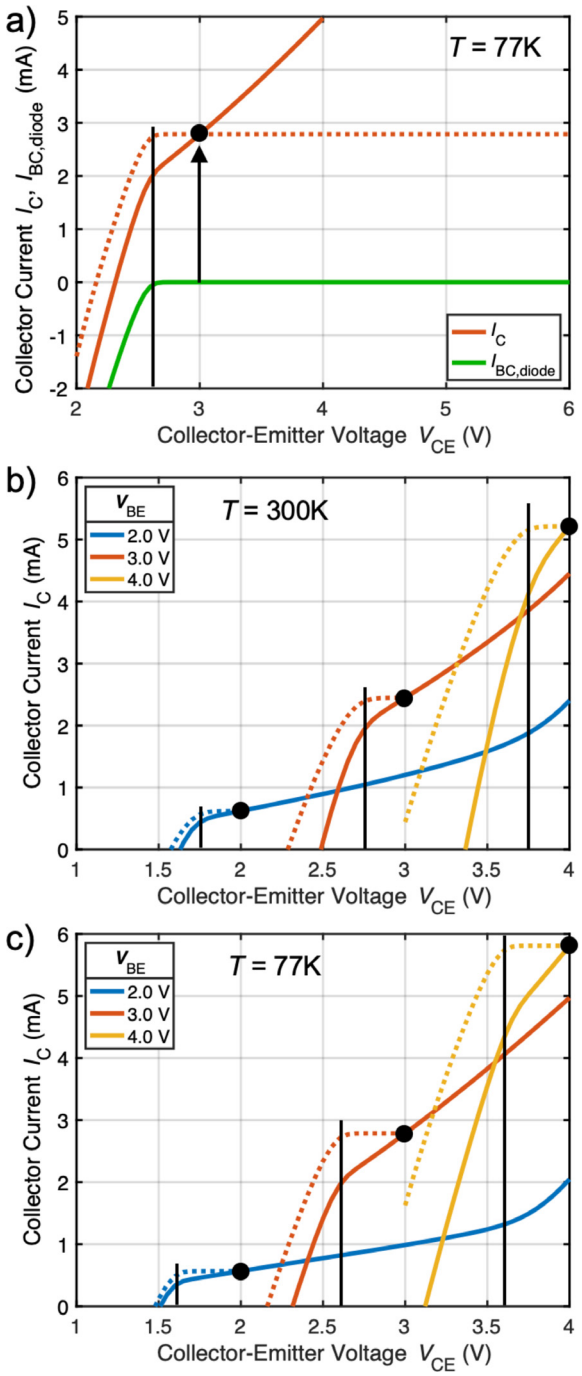

FIG. 5. (a) Common-emitter I_C–V_{CE} of device T1 for $V_{BE} = 3$ V (orange), with the $I_{BC,diode}$–V_{CB} (green) and the same $I_{BC,diode}$–V_{CB} curve shifted to the Gummel point (dashed orange) to illustrate BC diode contribution; (b) common-emitter characteristics for device T1 at 300 K for $V_{BE} = 2$, 3, and 4 V as a function of V_{CE} with $I_{BC,diode}$–V_{CB} (dotted), offset for each V_{BE} value to intersect at the Gummel point $V_{CB} = 0$ (circles); and (c) common-emitter characteristics for device T1 at 77 K for $V_{BE} = 2$, 3, and 4 V as a function of V_{CE} with BC diode contribution shown (dotted), offset to match the V_{CB} of each common-emitter curve and intersect at the Gummel points $V_{CB} = 0$ (circles).

improved gain, leading to a demonstration of collector current density >3 MA/cm^2 in our devices.

DISTRIBUTION STATEMENT A. Approved for public release. Distribution is unlimited. This material is based upon work supported by the Under Secretary of Defense for Research and Engineering under Air Force Contract No. FA8702-15-D-0001. Any opinions, findings, conclusions or recommendations expressed in this material are those of the author(s) and do not necessarily reflect the views of the Under Secretary of Defense for Research and Engineering. The lead author acknowledges the support of the Lincoln Scholars Program during his Brown Ph.D. studies. The authors would like to thank G. W. Turner for useful discussions.

AUTHOR DECLARATIONS

Conflict of Interest

The authors have no conflicts to disclose.

Author Contributions

J. W. Daulton: Conceptualization (lead); Data curation (lead); Formal analysis (lead); Funding acquisition (lead); Investigation (lead); Methodology (lead); Project administration (lead); Resources (lead); Writing – original draft (lead); Writing – review & editing (equal). **R. J. Molnar:** Investigation (supporting); Methodology (equal); Resources (equal). **J. A. Brinkerhoff:** Investigation (supporting); Methodology (supporting); Resources (supporting). **T. J. Weir:** Investigation (supporting); Methodology (equal); Resources (supporting). **M. A. Hollis:** Conceptualization (supporting); Formal analysis (supporting); Investigation (supporting); Methodology (supporting); Project administration (equal); Supervision (equal); Writing – review & editing (supporting). **A. Zaslavsky:** Conceptualization (equal); Methodology (supporting); Project administration (equal); Supervision (equal); Writing – review & editing (equal).

DATA AVAILABILITY

The data that support the findings of this study are available from the corresponding author upon reasonable request.

REFERENCES

[1]M. A. Hollis, S. C. Palmateer, L. F. Eastman, N. V. Dandekar, and P. M. Smith, "Importance of electron scattering with coupled plasmon-optical phonon modes in GaAs planar-doped barrier transistors," IEEE Electron Device Lett. **4**, 440 (1983).
[2]M. Heiblum, D. C. Thomas, C. M. Knoedler, and M. I. Nathan, "Tunneling hot-electron transfer amplifier: A hot-electron GaAs device with current gain," Appl. Phys. Lett. **47**, 1105 (1985).
[3]J. R. Hayes, A. F. J. Levi, and W. Wiegmann, "Hot-electron spectroscopy of GaAs," Phys. Rev. Lett. **54**, 1570 (1985).
[4]C.-Y. Chang, W. C. Lu, M. S. Jame, Y. H. Wang, S. Luryi, and S. M. Sze, "Induced base transistor fabricated by molecular beam epitaxy," IEEE Electron Device Lett. **7**, 497 (1986).
[5]A. Seabaugh, Y.-C. Kao, J. Randall, W. Frensley, and A. Khatibzadeh, "Room temperature hot electron transistors with InAs-notched resonant-tunneling-diode injector," Jpn. J. Appl. Phys. **30**, 921 (1991).
[6]M. S. Shur, A. D. Bykhovski, R. Gaska, M. A. Khan, and J. W. Wang, "AlGaN-GaN-AlInGaN induced base transistor," Appl. Phys. Lett. **76**, 3298 (2000).
[7]G. Gupta, M. Laurent, H. Li, D. J. Suntrup, E. Acuna, S. Keller, and U. K. Mishra, "Design space of III-N hot electron transistors using AlGaN and InGaN polarization-dipole barriers," IEEE Electron Device Lett. **36**, 23 (2015).

[8]Z. C. Yang, Y. Zhang, S. Krishnamoorthy, D. N. Nath, J. B. Khurgin, and S. Rajan, "Current gain above 10 in sub-10 nm base III-nitride tunneling hot electron transistors with GaN/AlN emitter," Appl. Phys. Lett. **108**, 192101 (2016).
[9]G. Gupta, E. Ahmadi, D. J. Suntrup III, and U. K. Mishra, "Establishment of design space for high current gain in III-N hot electron transistors," Semicond. Sci. Technol. **33**, 015018 (2018).
[10]D. J. Suntrup III, G. Gupta, H. Li, S. Keller, and U. K. Mishra, "Measuring the signature of bias and temperature-dependent barrier heights in III-N materials using a hot electron transistor," Semicond. Sci. Technol. **30**, 105003 (2015).
[11]C. Zeng, E. B. Song, M. Wang, S. Lee, C. M. Torres, Jr., J. Tang, B. H. Weiller, and K. L. Wang, "Vertical graphene-base hot-electron transistor," Nano Lett. **13**, 2370 (2013).
[12]A. Zubair, A. Nourbakhsh, J.-Y. Hong, M. Qi, Y. Song, D. Jena, J. Kong, M. Dresselhaus, and T. Palacios, "Hot electron transistor with van der Waals base-collector heterojunction and high-performance GaN emitter," Nano Lett. **17**, 3089 (2017).
[13]F. Giannazzo, G. Greco, E. Schilirò, R. Lo Nigro, I. Deretzis, A. La Magna, F. Roccaforte, F. Iucolano, S. Ravesi, E. Frayssinet, A. Michon, and Y. Cordier, "High-performance graphene/AlGaN/GaN Schottky junctions for hot electron transistors," ACS Appl. Electron. Mater. **1**, 2342 (2019).
[14]J. W. Daulton, R. J. Molnar, J. A. Brinkerhoff, M. A. Hollis, and A. Zaslavsky, "III-nitride vertical hot electron transistor with polarization doping and collimated injection," Appl. Phys. Lett. **121**, 223503 (2022).
[15]J. W. Daulton, R. J. Molnar, J. A. Brinkerhoff, Z. C. Adamson, M. A. Hollis, and A. Zaslavsky, "GaN hot electron transistors: From ballistic to coherent," Solid-State Electron. **208**, 108741 (2023).
[16]See https://www.synopsys.com/silicon/tcad/device-simulation/sentaurus-device.html for "Synopsys Sentaurus Version 2020.06" (2020).
[17]J. W. Daulton, R. J. Molnar, and D. M. Lennon, "Selectivity control in AlGaN/GaN atomic layer etching," in AVS Atomic Layer Etching Workshop, 2015.
[18]M. Wohlfahrt, M. J. Uren, Y. Yin, K. B. Lee, and M. Kuball, "Vertical field inhomogeneity associated with threading dislocations in GaN high electron mobility transistor epitaxial stacks," Appl. Phys. Lett. **119**, 243502 (2021).
[19]M. Heiblum, E. Calleja, I. M. Anderson, W. P. Dumke, C. M. Knoedler, and L. Osterling, "Evidence of hot-electron transfer into an upper valley in GaAs," Phys. Rev. Lett. **56**, 2854 (1986).
[20]C. R. Crowell and S. M. Sze, "Ballistic mean free path measurements of hot electrons in Au films," Phys. Rev. Lett. **15**, 659 (1965).
[21]J. Hayes and A. F. J. Levi, "Dynamics of extreme nonequilibrium electron transport in GaAs," IEEE J. Quantum Electron. **22**, 1744 (1986).
[22]E. M. Conwell, *High Field Transport in Semiconductors* (Academic Press, New York, 1967), pp. 149–160.
[23]J. W. P. Hsu, M. J. Manfra, D. V. Lang, S. Richter, S. N. G. Chu, A. M. Sergent, R. N. Kleiman, L. N. Pfeiffer, and R. J. Molnar, "Inhomogeneous spatial distribution of reverse bias leakage in GaN Schottky diodes," Appl. Phys. Lett. **78**, 1685 (2001).
[24]B. S. Simpkins, E. T. Yu, P. Waltereit, and J. S. Speck, "Correlated scanning Kelvin probe and conductive atomic force microscopy studies of dislocations in gallium nitride," J. Appl. Phys. **94**, 1448 (2003).
[25]E. J. Tarsa, B. Heying, X. H. Wu, P. Fini, S. P. DenBaars, and J. S. Speck, "Homoepitaxial growth of GaN under Ga-stable and N-stable conditions by plasma-assisted molecular beam epitaxy," J. Appl. Phys. **82**, 5472 (1997).
[26]F. C.-P. Massabuau, S. L. Rhode, M. K. Horton, T. J. O'Hanlon, A. Kovács, M. S. Zielinski, M. J. Kappers, R. E. Dunin-Borkowski, C. J. Humphreys, and R. A. Oliver, "Dislocations in AlGaN: Core structure, atom segregation, and optical properties," Nano Lett. **17**, 4846 (2017).
[27]D. A. Browne, M. N. Fireman, B. Mazumder, L. Y. Kuritzky, Y.-R. Wu, and J. S. Speck, "Vertical transport through AlGaN barriers in heterostructures grown by ammonia molecular beam epitaxy and metalorganic chemical vapor deposition," Semicond. Sci. Technol. **32**, 025010 (2017).
[28]E. Ahmadi, H. Chalabi, S. W. Kaun, R. Shivaraman, J. S. Speck, and U. K. Mishra, "Contribution of alloy clustering to limiting the two-dimensional electron gas mobility in AlGaN/GaN and InAlN/GaN heterostructures: Theory and experiment," J. Appl. Phys. **116**, 133702 (2014).
[29]I. Bryan, Z. Bryan, S. Mita, A. Rice, L. Hussey, C. Shelton, J. Tweedie, J.-P. Maria, R. Collazo, and Z. Sitar, "The role of surface kinetics on composition and quality of AlGaN," J. Cryst. Growth **451**, 65 (2016).
[30]R. J. E. Jansen, B. Farid, and M. J. Kelly, "Angular dependence of hot-electron transport through a two-dimensional electron-gas layer," Phys. Rev. B **47**, 13401 (1993).
[31]C. Liu, G. Zhao, G. Liu, Y. Song, H. Zhang, D. Jin, Z. Li, X. Liu, S. Yang, Q. Zhu, and Z. Wang, "Scattering due to large cluster embedded in quantum wells," Appl. Phys. Lett. **102**, 052105 (2013).
[32]A. A. Grinberg and S. Luryi, "Ballistic versus diffusive base transport in the high-frequency characteristics of bipolar transistors," Appl. Phys. Lett. **60**, 2770 (1992).
[33]Z. Lochner, H. J. Kim, Y.-C. Lee, Y. Zhang, S. Choi, S.-C. Shen, P. D. Yoder, J.-H. Ryou, and R. D. Dupuis, "NpN-GaN/$In_xGa_{1-x}N$/GaN heterojunction bipolar transistor on free-standing GaN substrate," Appl. Phys. Lett. **99**, 193501 (2011).
[34]V. A. Jhalani, J.-J. Zhou, and M. Bernardi, "Ultrafast hot carrier dynamics in GaN and its impact on the efficiency droop," Nano Lett. **17**, 5012 (2017).
[35]S. Luryi, "Quantum capacitance devices," Appl. Phys. Lett. **52**, 501 (1988).